ARTICLE NO. 80-4000

J80-008

MHD Boundary Layer of the Seeded Combustion Gas near Cold Electrodes

10015
20011

Ken Okazaki,* Yasuo Mori,† Kunio Hijikata,‡ and Kazutomo Ohtake‡
Tokyo Institute of Technology, Tokyo, Japan

A theoretical analysis of the seeded combustion gas boundary layer near cold electrodes was made under the magnetic field, and the effects of the magnetic field on various physical quantities in the boundary layer and the stability of current discharge of diffuse mode were clarified. First, a boundary-layer analysis was done using a three-fluid model that considered the phenomena near cold electrodes such as charge separation, electron temperature elevation above gas temperature, and nonequilibrium of electron number density from the Saha equilibrium value for the electron temperature for both cases of a continuous Faraday electrode and an ideally segmented Faraday electrode. It was shown that, in the case of an ideally segmented Faraday electrode, the nonequilibrium of electron number density for the Saha equilibrium value for the electron temperature became larger due to the magnetic field in the laminar boundary layer; whereas, Saha equilibrium of electron number density for the electron temperature was almost established in the turbulent boundary layer of practical MHD generators. Next, in order to investigate the effect of the magnetic field on the critical value of discharge mode from diffuse to constricted mode, an analysis of a linear stability theory was applied for a simplified model where the electron number density was given by the Saha equilibrium value for the gas temperature, the steady value of which was assumed uniform in the thin layer very near the cold electrode. It was made clear that a perturbed propagating wave was generated, and that discharge of diffuse mode would become very unstable because of the magnetic field.

Nomenclature

A_E = electric field coefficient defined by Eq. (34)
b^2 = discharge stability parameter
$\vec{B}$ = magnetic field vector [$\vec{B}=(0, 0, B)$]
$\vec{c}$ = phase velocity vector of perturbed wave [$\vec{c}=(c_x, c_y, c_z)$]
C_p = specific heat at constant pressure
e = electron charge
$\vec{E}$ = electric field vector [$\vec{E}=(E_x, E_y, E_z)$]
$\vec{\mathcal{E}}$ = generalized electric field [$\vec{\mathcal{E}}=(\mathcal{E}_x, \mathcal{E}_y, \mathcal{E}_z)$]
$\vec{J}$ = current density vector [$\vec{J}=(J_x, J_y, J_z)$]
k = Boltzmann's constant
$\vec{k}$ = nondimensional wave number vector [$\vec{k}=(k_x, k_y, k_z)$]
n = number density
P = pressure
Pr = Prandtl number
Q_{ex} = collision cross section for momentum exchange between electron and species X
Sc_i = Schmidt number of ion
t = time
T = gas temperature
T_e = electron temperature
$\vec{u}$ = mass average velocity vector [$\vec{u}=(u_x, u_y, u_z)$]
$\vec{u}_e, \vec{u}_i$ = velocity vectors of electron and ion
X = mole fraction
x,y,z = rectangular coordinates
β = Hall coefficient
δ = characteristic thickness of low electrical conductivity layer
δ_x = electron energy loss factor of species X
ϵ = permittivity of free space
η = nondimensional coordinate of y, y/δ
θ = nondimensional temperature or angle between x axis and the direction of perturbed wave
λ = thermal conductivity of gas
μ_e, μ_i = mobilities of electron and ion
ν = kinematic viscosity of gas
$\bar{\nu}_{ex}$ = averaged collision frequency between electron and species X
ρ = mass density
σ = scalar electrical conductivity
ϕ = electric potential
ψ = current stream function
ω = complex angular frequency

Subscripts

cr = critical value
e = electron
i = ion
im = imaginary part
K = potassium atom
r = real part
s = Saha equilibrium value
w = wall or surface condition
X = species X except ion and electron
x,y,z = x,y,z components
0 = unperturbed steady value
1 = perturbed value
∞ = main flow condition
$*$ = complex conjugate

Superscripts

$(\dot{\ })$ = net production in unit volume and unit time
$(\hat{\ })$ = nondimensional amplitude of perturbed quantity
$(\tilde{\ })$ = transformed quantity in Eq. (69)

Received Dec. 12, 1978; revision received Aug. 22, 1979. Copyright © American Institute of Aeronautics and Astronautics, Inc., 1979. All rights reserved. Reprints of this article may be ordered from AIAA Special Publications, 1290 Avenue of the Americas, New York, N.Y. 10019. Order by Article No. at top of page. Member price $2.00 each, nonmember, $3.00 each. **Remittance must accompany order.**

Index categories: MHD; Plasma Dynamics and MHD.

*Graduate Student, Dept. of Physical Engineering.
†Professor, Dept. of Physical Engineering.
‡Associate Professor, Dept. of Physical Engineering.

I. Introduction

IN order to solve the serious problem of electrode lifetime for the practical uses of MHD power generation, the use of cold electrodes is under investigation. However, in the

potassium seeded combustion gas (the working fluid of an open-cycle MHD generator), dependency on the temperature of electrical conductivity is large and the electrical conductivity near the cold electrode is much lower than that of the main flow region. Therefore, the physical phenomena are uncertain when a large electric current flows through this cold boundary layer. The authors previosly reported[1] an analysis of the boundary layer of the seeded combustion gas around a cold anode when current was applied by an external electric field without a magnetic field by use of a three-fluid model (electron, ion, and neutral species) and excluding the conventional sheath assumptions.[2-4] The following points were made clear concerning the cold electrode:

1) In an extremely large electric field near the electrode, an equilibrium of electron and gas temperatures is not realized, even with the combustion gas containing polyatomic molecules of large electron energy loss factor.

2) Ionization and recombination reactions are not sufficently fast, so the electron number density is much different from the Saha equilibrium value for an electron temperature.

3) Because the electric field intensity is very high near the electrode, an electron-ion charge separation occurs in a region much larger than the Debye length.

The authors[5] also reported an analysis of the instability of diffuse mode current discharge on the cold electrode surface by use of a linear stability theory for the case of no magnetic field.

In the present study, the former analyses are extended for the case of the magnetic field. First, a three-fluid model analysis of the seeded combustion gas boundary layer near cold electrodes is performed when the magnetic field is applied, taking phenomena peculiar to the cold electrode into consideration. For the cases of both continuous Faraday and ideally segmented Faraday electrodes, distributions of various physical quantities under the steady condition of diffuse mode discharge are made clear and effects of the magnetic field are clarified. Next, a linear stability theory is applied to a simplified model[5] in which electron number density is given by a Saha equilibrium value for the gas temperature, whose steady value is assumed constant in the thin layer very near the cold electrode, and the effects of the magnetic field on the critical condition of diffuse mode discharge are determined by use of a traveling wave of perturbed quantities.

II. Boundary Layer Analysis

A. Basic Equations

The field that was analyzed is shown in Fig. 1, together with the rectangular coordinate system, where x is the distance from the leading edge in the flow direction, y is the distance from the electrode surface perpendicular to it, and the z axis is normal to the x and y axes. As a basic research for the study of MHD boundary layer, a steady laminar boundary layer is first assumed on a cold flat-plate anode under the condition corresponding to the previous report[1]; afterwards a discussion about a turbulent boundary layer in practical MHD generators is considered. There is an external magnetic field in the z direction. In the main flow, the gas velocity and gas temperature are assumed constant along the flow direction. The magnetic Reynolds number is sufficiently small and, for simplicity, the density ρ, viscosity μ, thermal conductivity λ of the gas, and electron and ion mobilities μ_e and μ_i are assumed constant. This assumption of constant property is confirmed to have little essential effect on the results. In this case the fundamental equations by the three-fluid model (ion, electron, and neutral species)[1] under the magnetic field are as follows:

Overall continuity equation:

$$\frac{\partial u}{\partial x}+\frac{\partial v}{\partial y}=0 \tag{1}$$

Overall momentum equation:

$$u\frac{\partial u}{\partial x}+v\frac{\partial u}{\partial y}=\nu\frac{\partial^2 u}{\partial y^2}-\frac{1}{\rho}\frac{\partial P}{\partial x}+\frac{1}{\rho}J_yB \tag{2}$$

Overall energy equation:

$$u\frac{\partial T}{\partial x}+v\frac{\partial T}{\partial y}=\frac{\lambda}{\rho C_p}\frac{\partial^2 T}{\partial y^2}+\frac{1}{\rho C_p}\vec{J}\cdot\vec{E}' \tag{3}$$

Electron continuity equation:

$$\nabla\cdot(n_e\vec{u}_e)=\dot{n}_e \tag{4}$$

Ion continuity equation:

$$\nabla\cdot(n_i\vec{u}_i)=\dot{n}_i \tag{5}$$

Poisson's equation:

$$\nabla\cdot\vec{E}=(e/\epsilon)(n_i-n_e) \tag{6}$$

Electron energy equation:

$$\vec{J}\cdot\vec{E}'=\sum_x\delta_x\bar{\nu}_{ex}n_e(3/2)k(T_e-T) \tag{7}$$

Maxwell's equation:

$$\nabla\times\vec{E}=0 \tag{8}$$

In Eq. (7), because of the low electron number density, the fairly large electric field in the cold zone of the boundary layer near the electrode, and the extremely large electron energy loss factor associated with the electron/heavy-particle collision in the combustion gas, the dominant mechanism in the electron energy exchange is considered to be the local energy balance between the energy gained from the electric field and the energy loss by inelastic collisions with heavy particles.

The electron and ion fluxes in Eqs. (4) and (5) are expressed as follows, respectively, when the magnetic field is applied.

$$n_e\vec{u}_e=n_e\left[\vec{u}-\frac{\mu_e}{1+\beta_e^2}(I+\beta_eM_2)\cdot\vec{\mathcal{E}}_e\right] \tag{9}$$

$$\eta_i\vec{u}_i=n_i\left[\vec{u}+\frac{\mu_i}{1+\beta_i^2}(I-\beta_iM_i)\cdot\vec{\mathcal{E}}_i\right] \tag{10}$$

where

$$\beta_e=\mu_eB,\quad \beta_i=\mu_iB \tag{11}$$

are electron and ion Hall coefficients, respectively, and the components of tensors I, M_e, M_i are expressed as follows, respectively.

$$I=\begin{bmatrix}1&0&0\\0&1&0\\0&0&1\end{bmatrix}\quad M_e=\begin{bmatrix}0&-1&0\\1&0&0\\0&0&\beta_e\end{bmatrix}\quad M_i=\begin{bmatrix}0&-1&0\\1&0&0\\0&0&-\beta_i\end{bmatrix} \tag{12}$$

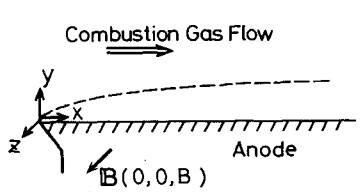

Fig. 1 Coordinate system.

Further, $\vec{\mathcal{E}}_e$, $\vec{\mathcal{E}}_i$ are generalized electric fields[6] and are expressed as follows:

$$\vec{\mathcal{E}}_e = \vec{E}' + (kT_e/en_e)\nabla n_e \tag{13}$$

$$\vec{\mathcal{E}}_i = \vec{E}' - (kT/en_i)\nabla n_i \tag{14}$$

where $\vec{E}'$ is expressed as follows in the sum of the external and induced electric fields:

$$\vec{E}' = \vec{E} + \vec{u} \times \vec{B} \tag{15}$$

Before solving Eqs. (4-10) about the electric and magnetic fields, several simplifications have to be made. The equation obtained by inserting Eq. (9) into Eq. (4) and dividing by $\mu_e/(1+\beta_e^2)$, and that obtained by inserting Eq. (10) into Eq. (5) and dividing by $\mu_i/(1+\beta_i^2)$ are added, and using $\vec{J} = e(n_i\vec{u}_i - n_e\vec{u}_e)$ and

$$\mu_i \ll \mu_e, \quad \beta_e \ll \beta_e \sim 1 \tag{16}$$

and replacing the charge separation term $(n_i - n_e)$ with $\nabla \cdot \vec{E}$ by Eq. (6), the following equation is obtained:

$$\vec{u} \cdot \nabla n_e + \nabla \cdot [(\epsilon\mu_i/e)(\nabla \cdot \vec{E})\vec{E}' - (\nu/Sc_i)(1 + T_e/T)\nabla n_e] - \nabla \cdot [\mu_i \beta_e n_e M_e \cdot \vec{\mathcal{E}}_e] = \dot{n}_e \tag{17}$$

Here Sc_i is the Schmidt number of ion in the gas. The production term $\dot{n}_e$ is expressed as

$$\dot{n}_e = (\alpha_e + \alpha_x) \cdot (n_{es}^2 - n_e n_i)$$

where α_e, α_x are recombination coefficients[1] when the third body is an electron or a heavy particle, respectively. In appearance Eq. (17) takes the form of an electron conservation equation, but as seen from the fact that the drift term is expressed by μ_i and not by μ_e, it is a fundamental equation to determine the electron concentration by movement of ion that shows slow correspondence to the electric field. The convective and diffusive terms of space charge are omitted since they are known to be small.[1] The last term on the left-hand side of Eq. (17) is the term newly introduced by the magnetic field.

Next, subtracting Eq. (4) from Eq. (5) and using $\dot{n}_e = \dot{n}_i$, we get

$$\nabla \cdot \vec{J} = 0 \tag{18}$$

From Eqs. (9), (10), and (16) and using the fact that the electron drift flux by the electric field is predominant among various fluxes of electron and ion for the large current density, the following equation is obtained:

$$\vec{J} = \frac{en_e\mu_e}{1+\beta_e^2}(I + \beta_e M_e) \cdot \vec{E}' \tag{19}$$

This approximate generalized Ohm's equation (19) is used only when $\vec{E}$ in Eq. (17) is estimated.

Thus Eqs. (6-8) and (17-19) are obtained to form the seven closed fundamental equations instead of Eqs. (4-10) to calculate seven variables of n_e, n_i, T_e, J_x, J_y, E_x, and E_y. From the standpoint of the present analysis (treating the boundary layer around the cold anode where the electrical conductivity changes markedly with the distance from the surface), fundamental equations are more simplified.

Boundary Layer Approximation

In the two-dimensional field, if a stream function ψ related to the electric current is introduced to satisfy the following relation, Eq. (18) is satisfied.

$$J_x = \partial\psi/\partial y \tag{20}$$

$$J_y = -\partial\psi/\partial x \tag{21}$$

Further, as $\nabla \times (\vec{u} \times \vec{B}) = 0$, Eq. (8) is expressed as follows:

$$\partial E_y'/\partial x - \partial E_x'/\partial y = 0 \tag{22}$$

Equation (19) is expressed with the respective components as follows:

$$E_x' = (1/en_e\mu_e)(J_x + \beta_e J_y) \tag{23}$$

$$E_y' = (1/en_e\mu_e)(-\beta_e J_x + J_y) \tag{24}$$

Substituting these equations into Eq. (22), and expressing it by ψ using Eqs. (20) and (21), the following are obtained:

$$\frac{\partial^2\psi}{\partial x^2} + \frac{\partial^2\psi}{\partial y^2} - A_x\frac{\partial\psi}{\partial x} - A_y\frac{\partial\psi}{\partial y} + \beta_e A_y\frac{\partial\psi}{\partial x} - \beta_e A_x\frac{\partial\psi}{\partial y} = 0 \tag{25}$$

where

$$A_x = \partial \ln\sigma/\partial x, \quad A_y = \partial \ln\sigma/\partial y \tag{26}$$

and σ is the electrical conductivity. In the following analysis of boundary layer around the cold electrode, as the electrical conductivity changes noticeably through the thin layer, the following condition is satisfied:

$$A_x \ll A_y \tag{27}$$

From the above, Eq. (25) is expressed as follows:

$$\frac{\partial^2\psi}{\partial x^2} + \frac{\partial^2\psi}{\partial y^2} - A_y\frac{\partial\psi}{\partial y} + \beta_e A_y\frac{\partial\psi}{\partial x} = 0 \tag{28}$$

Here, a local similar assumption as follows is almost valid for the limiting cases described below:

$$\partial J_y/\partial x = 0 \tag{29}$$

From Eqs. (29) and (21), the following equation is obtained:

$$\partial^2\psi/\partial x^2 = 0 \tag{30}$$

On the other hand, differentiation of Eq. (18) by x and the use of Eq. (29) lead to

$$\partial J_x/\partial x = \partial^2\psi/\partial x\partial y = C(y) \tag{31}$$

If $C(y)$ in Eq. (31) takes a finite value, only such a solution that J_y monotonously decreases to the y direction is reasonable, but for such a finite space between the opposing electrodes the only reasonable solution is

$$C = 0 \quad \text{or} \quad \partial^2\psi/\partial x\partial y = 0 \tag{32}$$

By considering Eqs. (30) and (32) for Eq. (28), we have $\partial E_x'/\partial y = 0$ from Eq. (23). Then from the calculation to satisfy Eqs. (27) and (29), the following relations are obtained:

$$J_y = \text{const}, \quad E_x' = \text{const} \tag{33}$$

Electrode Configurations

In consideration of the electrode configurations of MHD generators, two extreme limiting cases are studied: the continuous Faraday electrode (not segmented) and the ideally segmented Faraday electrode (infinitely segmented). In the case of the continuous Faraday electrode, as $E_x' = E_x = 0$ on the electrode wall, from Eq. (33) $E_x' = 0$ is satisfied in the whole region. On the other hand, in the case of ideally

segmented Faraday electrode, as $\int_0^L J_x \mathrm{d}y = 0$ (L = duct width), E_x' is expressed as follows:

$$E_x' = A_E(\beta_e J_y/\sigma_\infty) \tag{34}$$

A_E is a parameter that includes the duct width and takes the value of $1 \sim 2$. Our present method of analysis is applicable regardless of the magnetic field direction, but from the standpoint of performing an analysis around an anode, the present discussion will be limited to the case of magnetic field in the negative z direction ($B<0$) and then the electromotive force is generated in the positive y direction.

Under the condition mentioned above and when the current density J_y is given, the following four cases can be considered.

$$\text{(i) } B=0,\quad E_x=0 \quad \text{(ii) } B=0,\quad E_x\neq 0$$

$$\text{(iii) } B\neq 0,\quad E_x'=0 \quad \text{(iv) } B\neq 0,\quad E_x\neq 0 \tag{35}$$

The outline of the electric current flow patterns for each case is shown in Fig. 2. Case (i) corresponds to that studied in the previous report,[1] where current flows by an externally applied voltage and without the magnetic field. In this case,

$$J_x=0,\quad J_y=\text{const}>0,\quad E_x=0,\quad E_y=J_y/\sigma \tag{36}$$

For Case (ii), J_x exists because of E_x, but as the conductivity in the boundary layer rapidly decreases near the electrode, the value of J_x greatly changes. Thus we have

$$J_x=\sigma E_x,\quad J_y=\text{const}>0,\quad E_x=\text{const}<0,\quad E_y=J_y/\sigma \tag{37}$$

Case (iii) corresponds to that of the continuous Faraday electrode of MHD generator, and we have

$$J_x=-\beta_e J_y,\quad J_y=\text{const}>0,\quad E_x'=0,$$

$$E_y'=(1+\beta_e^2)(J_y/\sigma) \tag{38}$$

and the current flow pattern is straight. Case (iv) corresponds to an ideally segmented Faraday electrode, and the electric current flow pattern has the shape of the combination of cases (ii) and (iii).

$$J_x=-\beta_e J_y+\sigma E_x',\qquad J_y=\text{const}>0$$

$$E_x'=\text{const}<0,\qquad E_y'=(1+\beta_e^2)(J_y/\sigma)-\beta_e E_x' \tag{39}$$

Nondimensional Fundamental Equations

First, the last term on the left side of Eq. (17), which includes the effect of the magnetic field, is expressed as follows by substituting Eq. (39) into it in consideration of $\vec{\mathcal{E}}_e \sim \vec{E}'$ and Eq. (22):

$$-\nabla\cdot[\mu_i\beta_e n_e M_e\cdot\vec{E}] = u_m(\partial n_e/\partial x)+v_m(\partial n_e/\partial y) \tag{40}$$

where

$$u_m=(1+\beta_e^2)\beta_e\mu_i J_y/e\mu_e n_e-\beta_e^2\mu_i E_x' \tag{41}$$

$$v_m=-\beta_e\mu_i E_x' \tag{42}$$

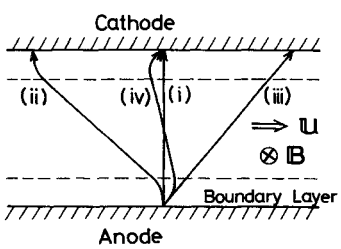

Fig. 2 Electrical current flow patterns.

This electron flux $n_e v_m$ is the y-direction flux generated by the interaction between the magnetic field and J_x, which changes to the y direction and will play a very important role in case (iv). Then Eqs. (17) and (7) are rewritten using given values of J_y and E_x' and are made nondimensional by the following coordinates:

$$\xi=x,\quad \eta_a=y\sqrt{u_\infty/2\nu x} \tag{43}$$

At the same time, the following nondimensionalizations are introduced.

$$f'=u/u_\infty,\quad \theta=T/T_\infty,\quad \theta_e=T_e/T_\infty,\quad \zeta=n_e/n_{e\infty} \tag{44}$$

By introducing the local similar assumption ($\partial/\partial\xi=0$), Eqs. (17) and (7) are expressed as follows, respectively.

$$(f+C_1)\zeta'+\{A_1(\zeta'/\zeta^3)+A_2(1+\theta_e/\theta)\zeta'\}'=-R \tag{45}$$

$$G_1(1/\zeta^2)=\sqrt{\theta_e}(\theta_e-\theta)/\theta \tag{46}$$

Here, a prime denotes differentiation with respect to η_a and

$$A_1=\frac{(1+\beta_e^2)^2\epsilon\mu_i J_y^2}{e^3\mu_e^2 n_{e\infty}^3}\cdot\frac{1}{\nu},\quad A_2=\frac{1}{Sc_i},\quad R=\frac{2\xi\dot{n}_e}{n_{e\infty}u_\infty}$$

$$C_1=\beta_e\sqrt{2\xi/u_\infty\nu}\;\mu_i E_x'$$

$$G_1=\frac{(1+\beta_e^2)J_y^2}{e\mu_e n_{e\infty}^2\cdot 2P\sqrt{\dfrac{8kT_\infty}{\pi m_e}}\displaystyle\sum_x\delta_x Q_{ex}X_x} \tag{47}$$

In Eqs. (45) and (46), only the predominating terms are left and several small terms arising from the space charge electric force are neglected. A_1 and G_1 are $(1+\beta_e^2)^2$ and $(1+\beta_e^2)$ times of those without magnetic field, respectively. C_1 newly comes from v_m of Eq. (42) and

$$C_1\propto J_y/\sqrt{u_\infty} \tag{48}$$

As for the flowfield, the case where the following equation is always effective in the momentum conservation equation (2) is considered, for simplicity.

$$\partial P/\partial x=J_y B \tag{49}$$

Then Eqs. (1-3) will be expressed as follows:

$$f'''+ff''=0 \tag{50}$$

$$\frac{1}{Pr}\theta''+f\theta'=-H\quad\left(H=\frac{2\xi}{\rho u_\infty C_p T_\infty}\cdot\frac{J^2}{e\mu_e n_{e\infty}\zeta}\right) \tag{51}$$

Boundary Conditions

The boundary conditions for Eqs. (45), (50), and (51) are

$$\eta\to\infty:\quad f'=1,\quad \theta=1,\quad \zeta=1 \tag{52}$$

$$\eta=0:\quad f=f'=0,\quad \theta=\theta_w=T_w/T_\infty$$

$$A_1(\zeta'/\zeta^3)+A_2(1+\theta_e/\theta)\zeta'=Z_1+Z_2\zeta \tag{53}$$

where

$$Z_1=\frac{(1+\beta_e^2)\mu_i J_y}{e\mu_e n_{e\infty}}\sqrt{\frac{2\xi}{u_\infty\nu}},\quad Z_2=-\beta_e\mu_i\sqrt{2\xi/u_\infty\nu}\,E_x' \tag{54}$$

The boundary condition, Eq. (53), is derived from the condition that ion flux should vanish on the anode surface.[1]

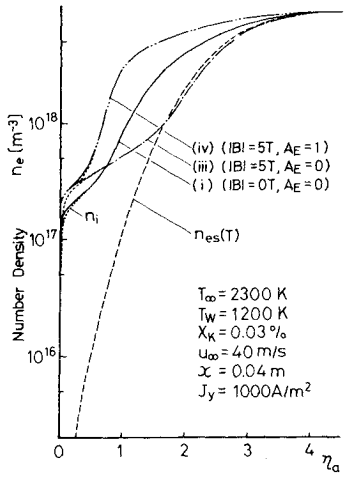

Fig. 3 Electron number density distributions in the laminar boundary layer.

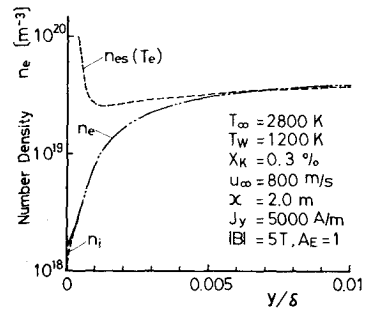

Fig. 4 Magnified structure of electron number density distributions very close to the cold anode in the turbulent boundary layer.

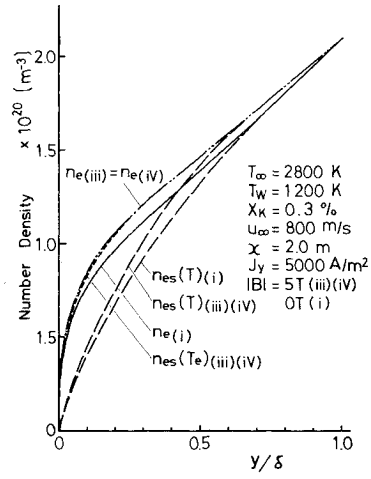

Fig. 5 Electron number density distributions in the turbulent boundary layer of practical MHD generators.

B. Results of Calculations and Discussions

As seen from Eqs. (45-47), in cases (i) and (ii) of Eq. (35) there is no difference in the fundamental equations; therefore, a solution without magnetic field is determined for case (i), then the effects of the magnetic field are investigated for cases (iii) and (iv). For the main flow temperature T_∞, the wall surface temperature T_w, potassium atom mole fraction X_K and the distance x from the leading edge, calculation conditions corresponding to those in the previous report[1] are taken. The results for $J_y = 1000$ A/m^2, $u_\infty = 40$ m/s, and $|B| = 5$ T is shown in Fig. 3. For case (iii) compared with case (i), the increase in thickness of the low electrical conductivity region or the charge separation region and the rise of electron number density near the electrode are caused by the decrease of the effective electrical conductivity to the y direction, which is reduced by the factor of $1/(1+\beta_e^2)$ due to the Hall effect seen from A_l and G_l of Eq. (47). In case (iv), because of E_x' and the extremely low electrical conductivity near the cold wall, J_x greatly changes to the y direction, as shown in Eq. (39) or Fig. 2 case (iv), and an eddy current remains as a result. Hence the electron flux $n_e v_m$ ($v_m < 0$) induced by the interaction of J_x and B is larger near the outer edge of the boundary layer than near the wall. The electron number density in the boundary layer then increases and the nonequilibrium state from the Saha equilibrium value becomes large and there is a large growth of the curve of electron number density in case (iv). This effect comes from the C_l term of Eq. (45), and is proportional to the factor $J_y/\sqrt{u_\infty}$, as seen from Eq. (48).

C. Turbulent Boundary Layer Analysis

The analytical method mentioned above is extended to an analysis of turbulent boundary layer in practical, open-cycle MHD generators. The analytical procedure is similar to that of the previous report.[1] Numerical results obtained are shown in Figs. 4 and 5. Figure 4 shows the magnified structure of electron number density distributions near the wall and charge separation is shown to be predominant only in the very thin region near the cold wall. However, as shown in Fig. 5, Saha equilibrium of electron number density for the electron temperature is almost established in the turbulent boundary layer of practical MHD generators. When the suffixes (i), (iii), and (iv) show the values given under the condition of Eq. (35), Fig. 5 shows that $n_{e(iii)}$ or $n_{e(iv)}$ is larger than $n_{e(i)}$ (because of the increase of Joule heating) by a factor of $1+\beta_e^2$ for a given J_y. However, the effect essential to magnetic field, expressed by the difference between $n_{e(iii)}$ and $n_{e(iv)}$, which is comparatively large for laminar flows as shown in Fig. 3, is seen negligibly small for turbulent flows.

Experimental data are not now available for comparison with these theoretical results. However, the elevation of nonequilibrium electron number density from the Saha equilibrium value for the gas temperature due to the large current density agrees qualitatively with the experimental results by Stanford.[7] It is hoped that more detailed experiments will be performed under a magnetic field for comparison with the results of this theory, taking nonequilibrium effects into consideration.

III. Analysis of Discharge Instability

A. Basic Equations

Discharge instability is controlled chiefly by the low electrical conductivity region near the cold electrode. A thin layer (thin region model[5]) of a characteristic thickness δ on the electrode surface is assumed, in which the electron number density is given by the Saha equilibrium value for the instantaneous gas temperature and convective effects are neglected. The magnetic Reynolds number is sufficiently small that the magnetic field is the imposed value. In the former report[5] a comparison between results based on this simplified model and those on a strict analysis taking the temperature distribution in account proves that there exists little difference in regard to the fundamental features. Under the conditions suggested above, fundamental equations for the unsteady and three-dimensional flow are expressed as follows for the coordinate system shown in Fig. 1 [with reference to Eqs. (3), (18), (8), and (19).]

Energy conservation equation:

$$\rho C_P \frac{\partial T}{\partial t} = \lambda \nabla^2 T + \vec{J}\cdot\vec{E} \tag{55}$$

Current conservation equation:

$$\nabla \cdot \vec{J} = 0 \tag{56}$$

Maxwell's equation:

$$\vec{E} = -\nabla\phi \quad (\nabla \times \vec{E} = 0) \tag{57}$$

Generalized Ohm's law:

$$\vec{J}=\frac{\sigma}{1+\beta_e^2}(I+\beta_e M_e)\cdot\vec{E} \tag{58}$$

Here, ϕ is an electrical potential, and I and M_e are given by Eq. (12). Equations (55-58) are reduced to eight equations consisting of a closed equation system to solve eight unknown quantities, $T,\phi,J_x,J_y,J_z,E_x,E_y$, and E_z. From these equations two equations for T and ϕ can be reduced. Equation (57) is substitutued into Eq. (58) to express $\vec{J}$ with ϕ, and substituting the equation thus obtained into Eqs. (55) and (56), Eqs. (55) and (56) are expressed as follows:

$$\rho C_P\frac{\partial T}{\partial t}=\lambda\left(\frac{\partial^2 T}{\partial x^2}+\frac{\partial^2 T}{\partial y^2}+\frac{\partial^2 T}{\partial z^2}\right)+\sigma\left[\frac{1}{1+\beta_e^2}\left\{\left(\frac{\partial\phi}{\partial x}\right)^2+\left(\frac{\partial\phi}{\partial y}\right)^2\right\}+\left(\frac{\partial\phi}{\partial z}\right)^2\right] \tag{59}$$

$$\frac{\partial^2\phi}{\partial x^2}+\frac{\partial^2\phi}{\partial y^2}+(1+\beta_e^2)\frac{\partial^2\phi}{\partial z^2}+\left(\frac{\partial\phi}{\partial x}-\beta_e\frac{\partial\phi}{\partial y}\right)\left(\frac{1}{\sigma}\frac{\partial\sigma}{\partial x}\right)+\left(\beta_e\frac{\partial\phi}{\partial x}+\frac{\partial\phi}{\partial y}\right)\left(\frac{1}{\sigma}\frac{\partial\sigma}{\partial y}\right)+(1+\beta_e^2)\frac{\partial\phi}{\partial z}\left(\frac{1}{\sigma}\frac{\partial\sigma}{\partial z}\right)=0 \tag{60}$$

Equations (59) and (60) are fundamental equations relating to T and ϕ, and the solutions are expressed as follows as the sum of the unperturbed steady term (subscript 0) and the perturbed term (subscript 1):

$$T=T_0+T_1,\quad \phi=\phi_0+\phi_1 \tag{61}$$

For simplification, T_0 is assumed constant in the layer in consideration, and as perturbed solution the following solutions are proposed:

$$T_1/T_\infty=\hat{T}(\eta)\exp[i\{k_x(x/\delta)+k_z(z/\delta)-\omega t\}] \tag{62}$$

$$\phi_1/(\delta J_{y0}/\sigma_\infty)=\hat{\phi}(\eta)\exp[i\{k_x(x/\delta)+k_z(z/\delta)-\omega t] \tag{63}$$

Here, k_x and k_z are wave numbers in the x and y direction, respectively, being nondimensionalized with the characteristic thickness δ.

Substituting Eq. (61) into Eqs. (59) and (60), linearizing small perturbed quantities, and making arrangements in consideration of Eqs. (62) and (63), the following two fundamental equations can be obtained for the nondimensional perturbed quantities $\hat{T}$ and $\hat{\phi}$:

$$\hat{T}^{**}-[(k_x^2+k_z^2)-\{(1+\beta_e^2)+A_E^2\beta_e^2S^2-2A_E\beta_e^2S\}b^2-ia]\hat{T}=\left(1-\frac{\beta_e^2}{1+\beta_e^2}A_ES\right)\gamma\hat{\phi}^*+\left\{\frac{\beta_e}{1+\beta_e^2}A_ES(ik_x)\right\}\gamma\hat{\phi} \tag{64}$$

$$\hat{\phi}^{**}-\{k_x^2+(1+\beta_e^2)k_z^2\}\hat{\phi}=(1+\beta_e^2)(2b^2/\gamma)\hat{T}^*+\beta_e(1+\beta_e^2)(A_ES-1)(2b^2/\gamma)(ik_x)\hat{T} \tag{65}$$

Here,

$$b^2=\frac{\delta^2J_{y0}^2}{\lambda\sigma_0T_0}\left(\frac{\partial\ln\sigma}{\partial\ln T}\right)_0,\quad \gamma=\frac{2\delta^2J_{y0}^2}{\lambda\sigma_\infty T_\infty},\quad a=\frac{\rho C_p}{\lambda}\omega\delta^2$$

and * expresses the differentiation with respect to η. σ_0 is the Saha equilibrium electrical conductivity for the gas temperature T_0, and $S=\sigma_0/\sigma_\infty\cdot b^2$ is a ratio of Joule heat to convective heat and is strongly related to the condition of discharge stability. A_E is a parameter given by Eq. (34). Now, if a condition of $S\ll 1$ is assumed, Eqs. (64) and (65) are expressed as follows for electrode configurations of either continuous Faraday or ideally segmented Faraday electrodes.

$$\hat{T}^{**}-\{(k_x^2+k_z^2)-(1+\beta_e^2)b^2-ia\}\hat{T}=\gamma\hat{\phi}^* \tag{66}$$

$$\hat{\phi}^{**}-\{k_x^2+(1+\beta_e^2)k_z^2\}\hat{\phi}=(1+\beta_e^2)(2b^2/\gamma)\hat{T}^*-\beta_e(1+\beta_e^2)(2b^2/\gamma)(ik_x)\hat{T} \tag{67}$$

For cases without a magnetic field ($\beta_e=0$), setting $k^2=k_x^2+k_z^2$, these equations are identical to those obtained for the thin region model in our previous report.[5] The term featuring the effect of the magnetic field is the second term of the right-hand side of Eq. (67). The principle of exchange of stability established for cases without magnetic field is not applicable to cases with the magnetic field. Consequently, it is necessary to take traveling waves into consideration for the perturbation fields. Each of $\hat{T}$, $\hat{\phi}$, k_x, k_z, and a is a complex number, but conditions of neutral stability in the sense of locality and time are to be investigated, and we set,

$$k_{x_{im}}=0,\quad k_{z_{im}}=0,\quad a_{im}=0 \tag{68a}$$

Under given boundary conditions, the condition that $\hat{T}$ and $\hat{\phi}$ are obtained as nontrivial solution should be considered as an eigenvalue problem in relation to

$$b^2,\quad k_{xr},\quad k_{zr},\quad a_r \tag{68b}$$

In Eqs. (68a) and (68b) the subscripts r and im express a real and imaginary part, respectively.

As it is very difficult to obtain exact solutions of Eqs. (66) and (67), the Galerkin method will be used in the following analysis. In order to apply the Galerkin method easily, the next transformation is made:

$$\tilde{\phi}=(2/\pi)\gamma\hat{\phi},\quad \tilde{T}=\hat{T},\quad \tilde{\eta}=(\pi/2)\eta$$
$$\tilde{b}^2=(4/\pi^2)b^2,\quad \tilde{a}_r=(4/\pi^2)a_r$$
$$\tilde{k}_{xr}^2=(4/\pi^2)k_{xr}^2,\quad \tilde{k}_{zr}^2=(4/\pi^2)k_{zr}^2 \tag{69}$$

Then Eqs. (66) and (67) are expressed as follows:

$$\tilde{T}''-\{\tilde{k}_{xr}^2+\tilde{k}_{zr}^2-(1+\beta_e^2)\tilde{b}^2-i\tilde{a}_r\}\tilde{T}=\tilde{\phi}' \tag{70}$$

$$\tilde{\phi}''-\{\tilde{k}_{xr}^2+(1+\beta_e^2)\tilde{k}_{zr}^2\}\tilde{\phi}=2(1+\beta_e^2)\tilde{b}^2\tilde{T}'-2\beta_e(1+\beta_e^2)\tilde{b}^2(i\tilde{k}_{xr})\tilde{T} \tag{71}$$

where the prime expresses the differentiation with respect to $\tilde{\eta}$. The boundary conditions are: on the outer edge of the layer no temperature and current density perturbation exists, and on the electrode surface, to assume good thermal and electrical conductivity, we also assume no perturbation of temperature and electrical potential. Then the following are given:

$$\tilde{\eta}=0:\quad \tilde{T}=0,\quad \tilde{\phi}=0 \tag{72}$$

$$\tilde{\eta}=\frac{\pi}{2}:\quad \tilde{T}=0,\quad \tilde{\phi}'+i\tilde{k}_{xr}\beta_e\tilde{\phi}=0 \tag{73}$$

B. Solution by the Galerkin Method

The distribution forms of the first perturbation satisfying the boundary conditions (72) and (73) are assumed as Eqs. (74) and (75). The aptness of this assumption has been con-

firmed by comparing the result with the exact solution[5] for $\beta_e = 0$.

$$\tilde{T} = c_1 \tilde{T}_1 + c_2 \tilde{T}_2 \tag{74}$$

$$\tilde{\phi} = d_1 \tilde{\phi}_1 + d_2 \tilde{\phi}_2 \tag{75}$$

where

$$\tilde{T}_1 = \sin 2\tilde{\eta}, \quad \tilde{T}_2 = \sin 4\tilde{\eta}$$

$$\tilde{\phi}_1 = \sin\tilde{\eta} \cdot \exp(-i\tilde{k}_{xr}\beta_e\tilde{\eta})$$

$$\tilde{\phi}_2 = \sin 3\tilde{\eta} \cdot \exp(-i\tilde{k}_{xr}\beta_e\tilde{\eta})$$

By substituting Eq. (74) into Eq. (70), multiplying the weights of $\tilde{T}_{1^*}$ and $\tilde{T}_{2^*}$, and integrating them over $\tilde{\eta} = 0 \sim \pi/2$; then substituting Eq. (75) into Eq. (71), multiplying the weights of $\tilde{\phi}_{1^*}$ and $\tilde{\phi}_{2^*}$, and integrating them over $\tilde{\eta} = 0 \sim \pi/2$, four simultaneous complex algebraical equations for c_1, c_2, d_1, and d_2 are obtained, where the subscript * expresses the complex conjugate. By setting the determinant of coefficient matrix of these simultaneous equations at zero, two equations to determine the eigenvalue relations can be obtained from the real and imaginary parts. That is, in the space of $\tilde{k}_{xr}$, $\tilde{k}_{zr}$ and $\tilde{b}^2$, a curved surface of neutral stability can be obtained, and on the respective point of the curved surface $\tilde{a}_r$ is determined. On the curved surface of neutral stability thus obtained, a perturbation corresponding to the point giving the minimum value of parameter $\tilde{b}^2$ (critical point) is most liable to occur. The propagation speeds of a perturbed wave nondimensionalized by the speed of the temperature propagation in the thickness of δ, $(\lambda/\rho C_p \delta)$, are expressed in the x and z directions, respectively, as:

$$c_x = a_r / k_{xr}, \quad c_z = a_r / k_{zr} \tag{76}$$

Assuming the angle of propagation velocity vector $\vec{c} = (c_x, c_z)$ to the x axis as θ, it is written as

$$\tan\theta = k_{zr} / k_{xr} \tag{77}$$

and the velocity is

$$c = a_r / \sqrt{k_{xr}^2 + k_{zr}^2} \tag{78}$$

Calculations to obtain the curved surface of neutral stability mentioned above are rather complicated, but can be obtained by numerically solving $\tilde{b}^2$ and $\tilde{a}_r$ using the Newton-Raphson method for values of $\tilde{k}_{xr}$ and $\tilde{k}_{zr}$.

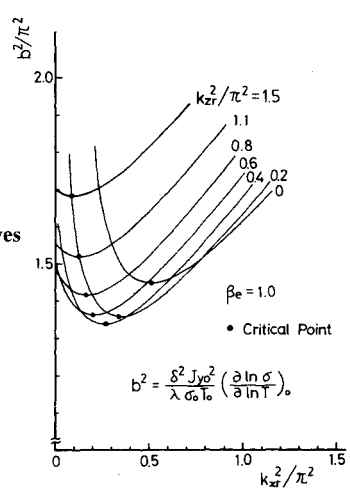

Fig. 6 Neutral stability curves on surfaces of k_{zr} = const.

C. Results and Discussion

The calculation results are expressed in terms of k_{xr}^2/π^2, k_{zr}^2/π^2, b^2/π^2, and a_r/π^2. Figure 6 shows an example of a neutral stability curves group in the case of $\beta_e = 1.0$ obtained by cutting the curved surface of neutral stability in the space of $k_{xr}^2 - k_{zr}^2 - b^2$. Similar figures can be drawn for various values of β_e. Figure 7 illustrates the critical points obtained above by taking $k_{cr}^2 = (k_{xr}^2)_{cr} + k_{zr}^2$ in the horizontal axis. When $\beta_e = 0$, both k_{cr}^2 and b_{cr}^2 become a constant value, and therefore is expressed as one point. In Fig. 7, the point making the value of b_{cr}^2 minimum is the critical point for the stability of diffuse mode discharge, and the value of b_{cr}^2 at this critical point with the magnetic field is much smaller compared with that without the magnetic field. This means that discharge is liable to be extremely unstable because of the magnetic field. From Fig. 7 it is also seen that when β_e is small, b_{cr}^2 becomes the minimum for $k_{zr}^2 = 0$, and perturbed waves propagate only in the x direction, but that when β_e is large, an extreme and minimum value of b_{cr}^2 is attained at

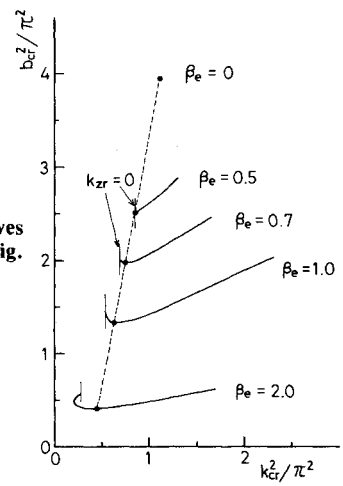

Fig. 7 Neutral stability curves made up by critical points in Fig. 6.

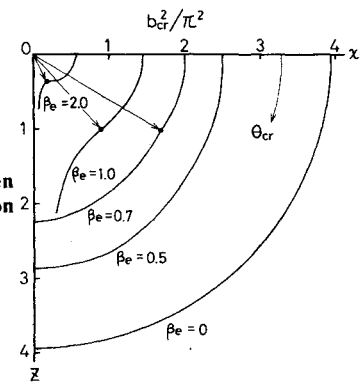

Fig. 8 Relation between critical value b_{cr}^2 and direction of perturbed wave.

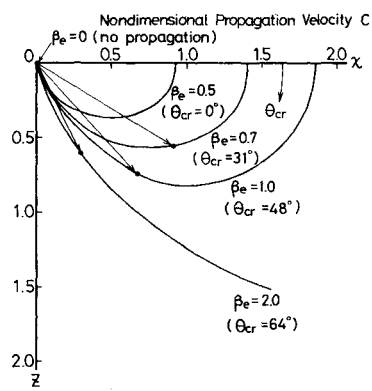

Fig. 9 Relation between nondimensional propagation velocity and direction of perturbed wave.

$k_{zr}^2 > 0$, and perturbed waves are most liable to generate and propagate in the direction to satisfy $\tan\theta_{cr} = (k_{zr})_{cr}/(k_{xr})_{cr}$. In order to clarify this phenomenon, the relation between the propagation direction θ_{cr} and the critical value of b_{cr}^2/π^2 for various β_e is shown in Fig. 8. The perturbed wave propagates in such a direction that b_{cr}^2 will become the minimum. When $\beta_e = 0$, the value of b_{cr}^2 is constant in all directions. When $\beta_e > 0$, the value of b_{cr}^2 varies with the direction. When β_e is small b_{cr}^2 is the minimum at $\theta_{cr} = 0$, but with and increase of β_e, θ_{cr} where b_{cr}^2 is the minimum becomes gradually large . The realtionship between the nondimensional propagation velocity c of this perturbed wave [expressed by Eq. (78)] and the propagation direction is studied, and the result is shown in Fig. 9. The most probable propagation direction and velocity of the perturbed wave are shown by black dots. When $\beta_e = 0$, $a_r = 0$, that is, $c = 0$, and we have a nonpropagating, standing wave. When $\beta_e > 0$, the perturbed wave becomes a traveling wave, but the propagation direction of the perturbed wave being most probably generated and the direction of the maximum propagation velocity are not always identical.

IV. Conclusions

First, an analysis is made using a three-fluid model on the seeded combustion gas boundary layer around the cold anode under the magnetic field, and the following conclusions are obtained for laminar flows (1 and 2) and for turbulent flows (3).

1) As the effective electrical conductivity in the vertical direction to the electrode surface is reduced to $1/(1+\beta_e^2)$ by the magnetic field, the region of small electron number density near the cold wall gets thicker, as does the charge separation region, compared with the case of no magnetic field.

2) In the case of the ideally segmented Faraday electrode, due to the generation of an eddy current in the boundary layer, nonequilibrium of electron number density from a Saha equilibrium value becomes large, and this effect is more important with the increase of current density and the decrease of main flow velocity.

3) In the turbulent boundary layer of practical MHD generators, the effect essential to a magnetic field as described in conclusion 2 is very small and the electron number density agrees with the Saha equilibrium value for the electron temperature through the boundary layer, excluding an extremely narrow region close to the cold electrode.

Second, another analysis is made on transition of discharge mode from diffuse to arc mode under the magnetic field by use of a linear stability theory, and the following conclusions are obtained.

4) The magnetic field greatly deteriorates the stability of diffuse mode discharge.

5) The perturbed wave being most probably generated is a nonpropagating, standing wave with no magnetic field, but is a propagating wave with the magnetic field.

6) Under the magnetic field, the propagation direction of the perturbed wave is almost perpendicular to the magnetic field when the magnetic field is weak, but it gradually turns to the direction of the magnetic field with an increase in strength of the magnetic field.

7) The propagating direction of the perturbed wave is not always identical with the direction of the maximum propagation velocity.

References

[1] Okazaki, K., Mori, Y., Ohtake, K., and Hijikata, K., "Analysis of the Seeded Combustion Gas Boundary Layer near a Cold Electrode," *AIAA Journal*, Vol. 15, Dec. 1977, pp. 1778-1784.

[2] Sherman, A., Yeh, H., Reshotko, E., and McAssay, E. Jr., "MHD Boundary Layers with Nonequilibrium Ionizational and Finite Rates," AIAA Paper 71-139, New York, 1971.

[3] Brown, R. T., "Electron Temperature and Number Density Measurements in a Nonequilibrium Plasma Boundary Layer," Institute of Plasma Research, Stanford University, Stanford, Calif., SU-IPR Report No. 350, Jan. 1970.

[4] Cotte, D. W., "Ionization and Electron Thermal Nonequilibrium in MHD Boundary Layers," *AIAA Journal*, Vol. 9, Dec. 1971, pp. 2404-2410.

[5] Okazaki, K., Mori, Y., Hijikata, K., and Ohtake, K., "Electrothermal Instability in the Seeded Combustion Gas Boundary Layer near Cold Electrodes," *AIAA Journal*, Vol. 16, April 1978, pp. 334-339.

[6] Mitchner, M. and Kruger, C. H., Jr., *Partially Ionized Gases*, Wiley, New York, 1973.

[7] James, R. K. and Kruger, C. H., "Boundary Layer Profile Measurements in the Electrode Wall of a Combustion Driven MHD Channel," *17th Symposium on Engineering Aspects of Magnetohydrodynamics*, Paper E.3, 1978, Stanford, Calif.